Journal of the European Ceramic Society **15** (1995) 95–99

0955-2219/95/$9.50

Oxygen Enrichment at Inversion Domain Boundaries in Aluminium Nitride—Influence on Thermal Conductivity

G. Gorzawski,[a,b] M. Sternitzke,[a] W. F. Müller,[b] A. Berger[c] & G. Müller[c]

[a] Fachbereich Materialwissenschaft and [b] Institut für Mineralogie, Technische Hochschule Darmstadt, D-642 87 Darmstadt, Germany
[c] Fraunhofer Institut für Silicatforschung, D-97082 Würzburg, Germany

(Received 10 December 1993; accepted 10 May 1994)

Abstract

Inversion domains (IDs) are a common feature in the microstructure of AlN ceramics. It is shown by transmission electron microscopy (TEM) that the frequency of IDs can be influenced to a large extent by processing and sintering parameters. Evidence is presented that the presence of IDs has a favourable effect on thermal conductivity. This is explained by oxygen trapping at the inversion domain boundaries (IDBs). Direct proof for the oxygen enrichment at the IDBs is given by electron energy-loss spectroscopy (EELS) in combination with TEM.

1 Introduction

High thermal conductivity makes AlN ceramics (wurtzite-type crystal structure with space group $P6_3mc$) an attractive material for electronics. Slack[1] reported that thermal conductivity decreases linearly by dissolution of oxygen in the lattice of AlN single crystals. Oxygen can be incorporated into the AlN lattice by the following reaction:

$$Al_2O_3 \Rightarrow 2Al_{Al} + [\ ]_{Al} + 3O_N$$

($[\ ]_{Al}$ denotes an aluminium vacancy). Besides other defects inversion domains (IDs) have been frequently observed within the grains of AlN ceramics.[2–5] The character of the inversion domain boundaries (IDBs), showing Al–Al or N–N bonds, suggests an incorporation of oxygen. In fact, energy dispersive X-ray analysis (EDX) by Westwood & Notis indicates the presence of oxygen at the IDBs.[5]

Transmission electron microscopy (TEM) contrast analysis of different defect structures has led to a model for nucleation of IDs. In previous papers a description of inversion domain nucleation in combination with dislocations has been given.[6,7] The aim of this work was to investigate the oxygen enrichment at IDBs and their influence on thermal conductivity of the ceramic. For this purpose, it was necessary to control the formation and growth of IDs during processing. The oxygen distribution across IDBs has been measured by electron energy-loss spectroscopy (EELS). EELS in combination with TEM allows the quantitative determination of the oxygen content in AlN with a high spatial resolution. This method has been applied to AlN ceramics in earlier investigations.[8,9]

2 Experimental

Two different AlN starting powders were used. Powder A (Grade B, H. C. Starck, Berlin, Germany) has a medium particle size of 1·3–2 μm and a total oxygen content of 1·8 wt%. Powder B (Grade F, Tokuyama Soda, Tokyo, Japan) has a medium particle size of 1·2 μm and a total oxygen content of 1 wt%. Mixtures of both AlN powders and Y_2O_3 powder (H. C. Starck, Berlin, Germany) were attrition milled using Al_2O_3 balls in isopropanol. Y_2O_3 is a usual sintering aid for AlN ceramics. Attrition milling time was varied between 30 min and 8 h and Y_2O_3 addition between 0 and 4 wt%. Cold isostatically pressed cylinders were sintered in a gas-pressure sintering furnace with graphite heating elements under a pressure of 0·2 MPa N_2. End temperatures ranged between 1750°C and 2000°C and sintering times between 30 min and 4 h.

Hot gas extraction analysis (TC-436, LECO Co., St. Joseph, MI, USA) was carried out for selective determination of lattice-dissolved oxygen and oxide-bound oxygen of AlN ceramics.[10] Thermal conductivity was measured by a comparative method according to DIN 51908. In this measuring technique a cylindrical shaped sample (d = 18 mm, h = 20 mm) is placed in series with a reference cylinder between two heat reservoirs at constant temperatures (20 and 40°C). Thermal conductivity is derived by measuring the thermal gradient in the reference sample. The measuring range is 10 to 200 W/(mK) with an accuracy of ~3%.

Starting powders and sintered samples were investigated by TEM (Model Philips CM12, Eindhoven, The Netherlands, with 120 kV acceleration voltage). About 1000 grains of each sample were examined in order to determine the fraction of grains that contains dislocations or IDs. For TEM investigations grains of the uncrushed starting powders were transferred from a suspension in ethanol to a copper grid covered with a C-film after ultrasonic treatment. Electron transparent samples of the compact ceramics were prepared by argon ion milling.

The TEM is equipped with a parallel electron energy-loss spectrometer (PEELS, Model 666, Gatan, Pleasanton, CA, USA) and a double tilt specimen holder cooled with liquid nitrogen (Model 636, Gatan). Cooling of the specimen was necessary to prevent contamination effects. The EELS measurements were all recorded using the convergent beam mode in the TEM to provide a high spatial resolution. The illumination half-angle was 7 mrad, the collection half-angle was in the range of 10 to 20 mrad, the integration time was 25 ms for the low loss spectra and 100 s for the core-loss spectra, and the probe current density was approximately 3×10^6 e^-/nm^2. The EELS measurements allow the quantitative determination of the concentration ratio of nitrogen and oxygen ([N]/[O]) and of the sample thickness.[8] The complex data acquisition and processing in EELS is described in the literature.[11,12] Concentration profiles were measured by recording EEL spectra of a series of spots on a line across the IDB. The distance from the spots to the IDB was determined using the measuring function of the TEM. A series of micrographs with different exposure times was taken to estimate the electron spot size. A plot of the reciprocal exposure time versus the radius of the spot led to a Gaussian distribution with a full width half maximum (FWHM) of 15 nm in one case and 20 nm in another.

Spontaneous growth of an oxide layer at room temperature in air has to be taken into account for quantitative measurements of oxygen concentrations. In an earlier paper a method has been reported that enables the determination of the thickness of such oxide layers. The [N]/[O] ratios can then be corrected for the influence of the oxide layer.[8]

3 Results and Discussion

3.1 Occurrence of IDs during ceramic processing

Investigations of the starting powders show the presence of dislocations in both AlN powders. 90% of the grains in powder A contain dislocations, generally with a high dislocation density. The dislocations are connected to hexagonal networks in approximately 1% of the grains. By contrast, less than 1% of the grains in powder B have dislocations. While no IDs were found in starting powder A, 1% of the grains of powder B, contain IDs. Powder B was used to investigate the influence of attrition milling time on the amount of grains containing dislocations. The results are plotted in Fig. 1. Obviously, longer times of attrition milling increase the number of dislocations in the starting powder. Cold isostatic pressing of the mixed powders does not change the defect structures.

The defect structure of AlN ceramics after sintering was also investigated. IDs can be observed in ceramics made from both starting powders. They are often connected with dislocations. The amount of IDs in the sintered ceramics using powder B depends on the attrition milling time of the powder mixtures and therefore on the amount of dislocations. A higher amount of dislocations in the starting powder yields a higher number of IDs in the ceramic, as shown in Fig. 1. Powder A initially contains many grains with dislocations, therefore IDs were always observed in the sintered ceramic.

The fraction of grains containing IDs in ceramics of powders A and B after 8 h attrition milling depends on sintering temperature and Y_2O_3 content.

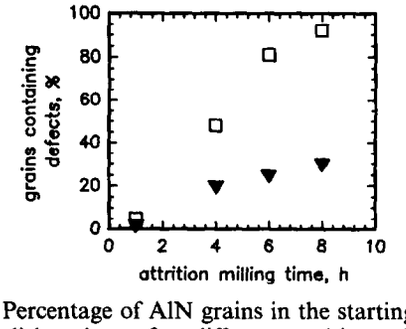

Fig. 1. □, Percentage of AlN grains in the starting powder B containing dislocations after different attrition milling times. The symbols ▼ represent the number of grains containing IDs of the sintered ceramics (1800°C).

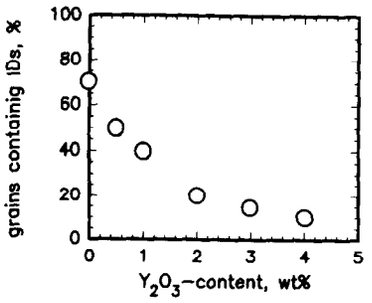

Fig. 2. Percentage of AlN grains containing IDs as a function of the Y_2O_3 content. The AlN ceramics were sintered at 1850°C for 1 h.

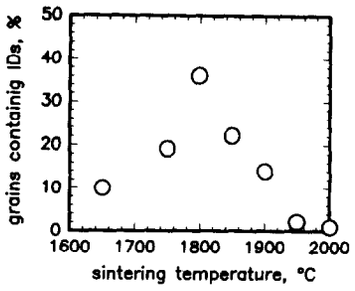

Fig. 3. Percentage of AlN grains containing IDs as a function of sintering temperature. The AlN ceramics were sintered with 2 wt% Y_2O_3 for 1 h.

Figure 2 shows the dependence of the number of IDs per 100 grains on Y_2O_3 content for a ceramic of powder A after sintering at 1850°C. As can be seen, the number of IDs decreases rapidly with an increasing Y_2O_3 content (Fig. 2). The correlation between IDs and temperature is presented in Fig. 3. A maximum of IDs is reached at 1800°C. The number of IDs drops to zero for the sintering temperature of 2000°C. Sintering time was investigated in the range between 30 and 240 min. For these sintering times no influence on the number of grains containing IDs has been found.

3.2 Thermal conductivity

Table 1 compares the oxygen content, number of IDs, and thermal conductivity of three pairs of differently sintered AlN ceramics. The difference between the two samples of each pair is that samples 1a, 2a and 3a were attrition milled for 1 h and samples 1b, 2b, and 3b, 6 h. Different dislocation densities in the powders and finally different numbers of IDs were found in each sample pair a and b (Table 1).

According to hot gas extraction analysis the powders take up oxygen during attrition milling. However, as can be seen in Table 1, milling time only increases the total oxygen concentration, not the lattice oxygen content. In the series of samples 1a to 3a and 1b to 3b thermal conductivity decreases. This is caused by an increase of the oxygen content dissolved in the AlN lattice. This in turn is a function of the Y_2O_3 content and the sintering conditions, as has been shown in several papers.[1,13]

There is no significant difference in lattice dissolved oxygen between samples a and b of each pair. However, thermal conductivity is always higher in sample a. This indicates that the presence of IDs has a favourable effect on thermal conductivity. This influence can be understood if indeed, as stated in the introduction, oxygen impurities are trapped at and dragged along with the IDBs. In this case the growth of the IDs would purify the interior of the IDs and thus increase their thermal conductivity. The IDs themselves must be supposed to be thermal conductivity barriers, but as they are very thin they probably are not very effective.[13] Oxygen segregated at the IDBs and oxygen dissolved in the AlN lattice cannot be distinguished by hot gas extraction analysis. Therefore, EELS in combination with TEM is necessary for a definite proof of the oxygen segregation at the IDBs.

The results described show the influence of IDs on thermal conductivity. Higher concentration of IDs increases the thermal conductivity. A low Y_2O_3 content is one condition to achieve a high concentration of IDs. However, a low oxygen content in the lattice resulting from high Y_2O_3 contents improve thermal conductivity. Therefore, the effect of improving thermal conductivity by IDs is contrary to the effect of high Y_2O_3 contents.

Table 1. Sintering and preparation conditions, oxygen contents, thermal conductivity and number of IDs for selected samples of powder B

Sample	*T (°C)*	*t (h)*	*Y_2O_3 (wt%)*	*Attrition milling (h)*	*$[O]_{total}$ (wt%)*	*$[O]_{lattice}$ (wt%)*	*Thermal conductivity (W/mK)*	*Number of IDs per 100 grains*
1a	1850	2	4	6	2·54 (5)	0·17 (5)	179 (6)	10
1b	1850	2	4	1	1·70 (5)	0·15 (5)	165 (6)	1
2a	1800	3	2	6	1·83 (5)	0·22 (5)	141 (6)	35
2b	1800	3	2	1	1·10 (5)	0·19 (5)	119 (6)	1
3a	1800	2	2	6	2·20 (5)	0·28 (5)	121 (6)	30
3b	1800	2	2	1	1·52 (5)	0·25 (5)	93 (6)	1

3.3 Oxygen enrichment at inversion domain boundaries

Figure 4(a) shows a TEM micrograph of an ID from sample 3a of Table 1. The end of the ID, where a planar and a curved IDB run close together, is shown. The planar IDB is oriented // (0001) in the AlN crystal. Figure 4 (b) gives the oxygen concentration profile measured by EELS across these two IDBs. Significantly increased oxygen concentrations with values of ~8 at.% at the IDBs have been found.

The width of the boundaries is small compared to the electron spot size of approximately 15 nm. The distance between the two IDBs is also 15 nm. The maximum of the profile in Fig. 4(b) therefore cannot be interpreted as the real oxygen concentration at the IDB. The measured oxygen concentration profile (Fig. 4(b)) represents the true oxygen distribution convoluted with the intensity distribution of the electron spot. A convenient method to interpret this type of profile, is the calculation of theoretical profiles and comparison to the measured one. The first step is to assume an ideal rectangular oxygen distribution. The oxygen incorporation at the IDBs can be described in terms of small oxygen layers similar to those in polytypes.[14] In the following calculations Al_2O_3 layers with an oxygen concentration of 60 at.% were assumed. High-resolution TEM investigations show that the width of an IDB is approximately 0·5–1 nm. These results agree with current studies.[15] Consequently, for the profile calculations a rectangular oxygen distribution with a width of 1·6 nm (two parallel IDBs) and a height of 60 at.% was convoluted with a Gaussian function (FWHM = 15 nm, diameter of the electron spot) and drawn in Fig. 4(b) as a solid line. The model corresponds reasonably with the measured data. However, the accuracy of the method is not sufficient to derive explicit values for the true oxygen concentration at the IDB.

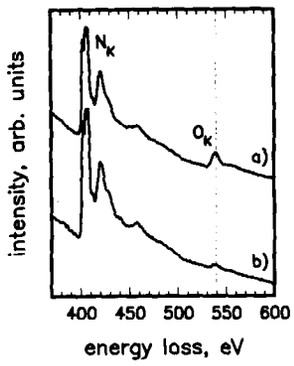

Fig. 5. EEL spectra measured (a) exactly at the IDB and (b) 35 nm beside the IDB. The EEL spectra include the characteristic N_K and O_K ionization edges.

Two typical EEL spectra are presented in Fig. 5. The range of energy loss is 370 to 600 eV including the N_K and O_K edges. The first EEL spectrum (a) was measured directly at the IDBs in Fig. 4 (x = 0). EEL spectrum (b) was recorded in a distance of 40 nm from the IDBs.

Figure 6(a) shows typical IDs of dome-like shape. A second EELS measurement (Fig. 6(b)) was obtained across one whole ID, including both the curved and planar boundary (see marks in Fig. 6(a)). The solid line in Fig. 6(b) was calcu-

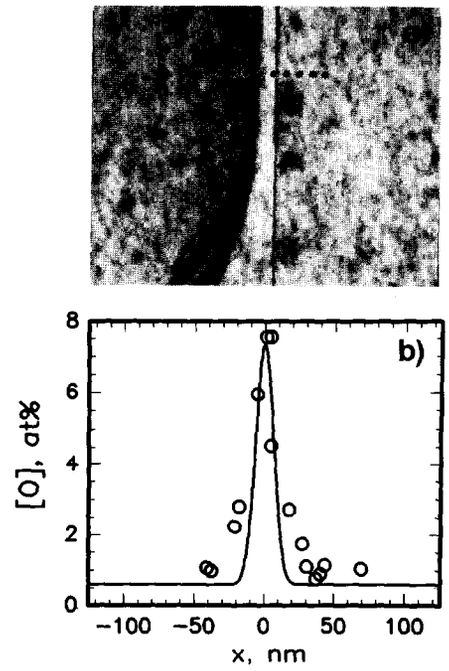

Fig. 4. (a) TEM micrograph of two IDBs. The primary beam is oriented // [$\bar{1}2\bar{1}0$]; (b) the oxygen concentration profile across the IDBs of (a) with the same scale.

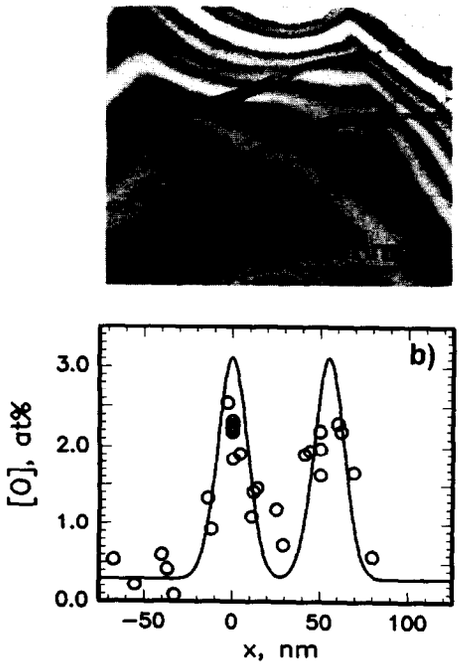

Fig. 6. (a) TEM micrograph of an AlN grain showing IDs. The primary beam is oriented // [$\bar{1}2\bar{1}0$]. (b) The oxygen concentration profile measured along the marked line.

lated using the same model as in the first example. In this case the width of each IDB amounts to 0·8 nm, the height to 60 at.% and the spatial resolution to 20 nm. The oxygen enrichment at the IDBs is again obvious.

4 Conclusions

It has been shown that the concentration of IDs in sintered AlN ceramics can be controlled by the powder processing and sintering parameters. The processing parameters chosen do not affect the total oxygen content within the AlN grains. Therefore, the influence of IDs on thermal conductivity can be evaluated directly. Evidence is presented that thermal conductivity increases with the concentration of IDs.

EELS in combination with TEM was successfully used to prove oxygen enrichment at IDBs. The improved thermal conductivity can be interpreted as an indirect result of this oxygen enrichment at the IDBs, if it is assumed that the lattice oxygen content is lowered inside the ID. This assumption has to be proved by further EELS measurements. In view of recent models[13] it seems reasonable that the positive effect on thermal conductivity resulting from the lower lattice oxygen content inside the ID overrides the negative influence of the oxygen enrichment at the narrow IDBs.

Acknowledgements

This work has been supported by the Deutsche Forschungsgemeinschaft, which is gratefully acknowledged. Thanks are also due to the Materials Research Department of Hoechst AG, Frankfurt, where the measurements of thermal conductivity have been made.

References

1. Slack, G. A., Nonmetallic crystals with high thermal conductivity. *J. Phys. Chem. Solids*, **34** (1973) 321–35.
2. Denanot, M. F. & Rabier, J., Characterisation of the microstructure of sintered AlN by transmission electron microscopy. *Mater. Sci. Engineering*, **A109** (1989) 157–160.
3. Hagege, S., Ishida, Y. & Tanaka, S., TEM analysis of impurity induced microstructures in sintered aluminium nitride ceramics. *Nippon Seramikkusu Kyokaki Gakujutsu Ronbunshi*, **92** (1988) 1119–26.
4. Berger, A., Inversion domains in aluminium nitride. *J. Am. Ceram. Soc.*, **74**(5) (1991) 1148–51.
5. Westwood, D. & Notis, M. R., Inversion domain boundaries in aluminium nitride. *J. Am. Ceram. Soc.*, **74**(6) (1991) 1226–39.
6. Berger, A., Nucleation and growth of inversion domains in AlN. Part I: Study of fundamental processes. *J. Am. Ceram. Soc.*, 1995.
7. Gorzawski, G., Weber, O., Berger, A. & Müller, W. F., Nucleation and growth of inversion domains in AlN. Part II: Study of advanced configurations. *J. Am. Ceram Soc.*, 1995.
8. Sternitzke, M., Growth of oxide layers on thin aluminum nitride samples measured by EELS. *J. Am. Ceram. Soc.*, **76**(9) (1993) 2289–94.
9. Sternitzke, M. & Müller, G., EELS study of oxygen diffusion in aluminum nitride. *J. Am. Ceram. Soc.*, **77**(3) (1994) 737–42.
10. Thomas, A. & Müller, G., Determination of the concentration of oxygen dissolved the AlN lattice by hot gas extraction from AlN ceramics. *J. Eur. Ceram. Soc.*, **8** (1991) 11–19.
11. Egerton, R. F., *Electron Energy-Loss Spectroscopy in the Electron Microscope*. Plenum Press, New York, 1986.
12. Disko, M. M., Ahn, C. C. & Fultz, B. (ed.), *Transmission Electron Energy Loss Spectrometry in Materials Science*. The Minerals, Metals and Materials Society, Warendale, PA, 1992.
13. Buhr, H. & Müller, G., Microstructure and thermal conductivity of AlN(Y_2O_3) ceramics sintered in different athmospheres. *J. Eur. Ceram. Soc.*, **12** (1993) 271–8.
14. Jack, K. H., Review—Sialons and related nitrogen ceramics. *J. Mat. Sci.*, **11** (1976) **11** 1135–58.
15. Ishida, Y., Hagege, S., Ichinose, H. & Takahashi, Y., High-resolution electron microscopy of ceramic interfaces. *J. Electr. Microsc, Techn.*, **12** (1989) 244–51.